Peer-reviewed version available at *Sensors* **2017**, *17*, 1701; doi:10.3390/s17081701

Article

Near-Infrared Spectroscopy-based Detector in Application of Intensive Care Unit Clinics

Ting Li *, Fulin Zhong, Zishan Deng, Boan Pan, Zebin Li

State Key Lab Elect Thin Film & Integrated Device, University of Electronic Science & Technology of China, Chengdu 610054, China; liting@uestc.edu.cn

* Correspondence: liting@uestc.edu.cn; Tel.: +86-151-9812-6481

Abstract: We attempted to apply the optoelectronic sensor entitled 'OPT101' in intensive care unit clinics, based on its optoelectronic response characteristics in near-infrared wavelength range and near-infrared spectroscopy principle. The successful novel applications in our lab include early-diagnosis and therapeutic effect tracking of thrombus, noninvasive monitoring of patients' shock severity, and fatigue evaluation. This study also expects further improvements of the detector in noninvasive clinical applications.

Keywords: optoelectronic sensor; near-infrared spectroscopy; thrombus diagnosis; shock monitoring; fatigue evaluation

1. Introduction

OPT101 is one type of optoelectronic sensor which convert optical signal into electronic signal with less noise [1] and signal amplification function. Currently, such and similar kind of optoelectronic sensor has been used for fruit or stem growth monitoring in agriculture [2], nitric oxide detection with high sensitivity [3], pulse oximetry for pulse rate and oxygenation measurement [4], and salivary diagnosis of stomach cancer [5]. These applications of OPT101 delights us that it might be a feasible choice as a detector in noninvasive clinical applications.

As we known, there is a demanding mission for developing noninvasive and sensitive monitoring techniques in intensive care unit (ICU), no matter for newborn babies or for emergency medication needed patients. Smart devices for diagnosis, monitoring, and therapeutic effect evaluation are specially needed. For examples, Shock resulting from trauma and hemorrhage often raise up fatal risk for patients, and the mortality rate is up to 50% [6, 7]. The salient killer deep vein thrombosis, as a fatal complication for old patients especially after surgery, may lead to a large range of high-incidence diseases related with heart and cerebral vessels [8]. Plus, the doctors and nurses usually suffered long-time and exhausting working, which may increase fatigue level and cause some undesirable accidents [9,10]. All of these requirements provided us the challenge to develop novel devices.

Near-infrared spectroscopy (NIRS), which wavelengths range from 700 nm to 900 nm, is a noninvasive, real-time and portable technique capable of continuously measuring hemodynamic variations in biological tissues [10,11]. The advantages of noninvasive monitoring, portability, and relatively small-size instrumentation make photoelectric sensor based NIRS to be a proper methodology for intensive care unit clinics (ICU). Here, we attempt to introduce an optoelectronic sensor to ICU. Compared to common care units of hospitals, ICU requires closer observation, more real-time/sensitive monitoring and even noninvasive measurements, allowing patients to get more intensive care and timely treatment. As an effective, nondestructive, and non-ionizing measurement technique, NIRS has attracted more and more researchers' attention. NIRS has been widely applied in various domains of science, including agriculture monitoring [12], food test [13], drug analysis [14], medical diagnosis [15], and etc., here we mainly focus on its successful applications in life science achieved by our group and collaborators.

Peer-reviewed version available at Sensors 2017, 17, 1701; doi:10.3390/s17081701

Here, we attempted to apply the optoelectronic sensor 'OPT101' in portable NIRS device design especially for ICU use. We mainly utilized 3-wavelengths (735 nm, 805 nm, and 850 nm) integrated LED as near-infrared light source and OPT101 as detector in our custom medical NIRS device. The optoelectronic response characteristics of OPT101 in near-infrared wavelength range (700~900 nm) and especially response to the utilized wavelengths in our custom NIRS device were analyzed. Plus, the feasibility of OPT 101 in sensing the signal in the measured tissue of human body was analyzed by realistic light propagation modeling. Then we reported the measurement algorithm for NIRS device to measure disease-sensitive hemodynamic parameters. After that, we reported some successful OPT101 embedded ICU-specific NIRS devices, including the one for early-diagnosis and therapeutic effect tracking of thrombus, noninvasive monitoring of shock patients' conditions, and the one for fatigue evaluation of long time working medical staffs [9,15,16,17]. Clinical experimental tests were carried out to fully test the reliabilities of these devices. Our data showed successful application of OPT101 in ICU-specific NIRS devices and the great potential of OPT101 in medicine and home healthcare.

2. Methods and Materials

2.1. Photoelectric Detector OPT101 and applicable probe design

The photoelectric detector OPT101 (Figure 1(a)), is a monolithic photodiode which output voltage response increases linearly along with the collected light intensity. This photoelectric sensor is equipped with a one-ship transimpedance amplifier for extracting weak signal and accordingly improve the effectiveness of data collection. OPT101 is sensitive to near-infrared light with wavelengths ranging from 700 nm to 900 nm, which is suitable for our application of recording light intensity variation at especially 735 nm, 805 nm, and 850 nm wavelengths. As shown in special responsivity curve in Figure 1(b), the values of responsivity at the utilized wavelengths are close to the peak value around 0.6, which benefit us to sense the light signal sensitively in our application.

Here, OPT101 was utilized to collect light intensity signals in a certain measurement site of human body and converted to electrical signals, such as voltage signal. The output voltage response was recorded, displayed, and analyzed in our custom software included in the developed NIRS device specific to intensive care unit clinics.

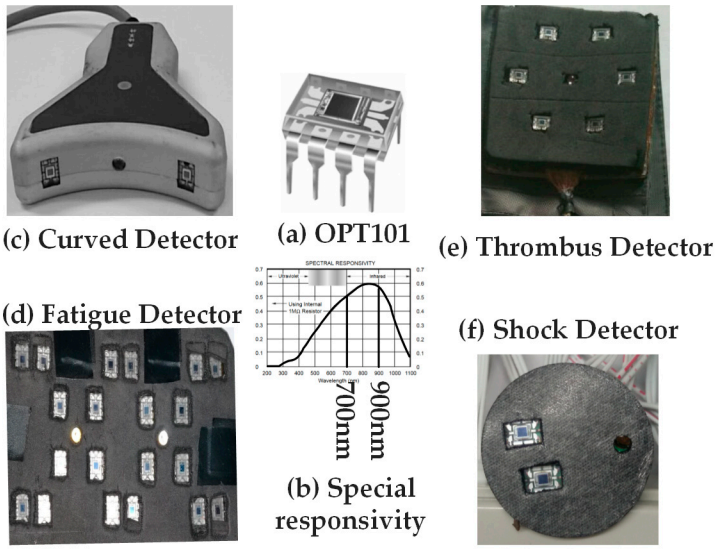

Figure 1. (**a**) OPT101 detector; (**b**) responsivity along with wavelength of OPT101; (**c-f**) the probe designs with the detector embedded according to different applications.

Figure 1(c-f) showed the probe designs with the optoelectronic detector imbedded, for the applications of handheld curved scanning health detector (c), thrombosis detector (d), fatigue monitor (e), and shock status reporter (f). The number of detectors, the separation between the light source and detector, and the placement of the light source and detectors were different among the

Peer-reviewed version available at Sensors 2017, 17, 1701; doi:10.3390/s17081701

above application, respective to measurement region geometry and measurement algorithm. For example, the handheld curved scanning health detector in Figure 1(c) was specially for measuring legs, arms, and breast with round-like geometry, thus the scanning touching surface was designed to be curved. The separation of light source and detector was 2.5 cm, which was the average optimized value applicable to the measured body tissue. Plus, this detector application is of relative bilateral comparison measurement, accordingly, the contralateral placement of the two OPT101 aside of the light source is employed.

The detector for thrombus, fatigue and shock were designed into a flexible printed circuit board with black blocking leather attached onto either sites, which allows the detector and detecting surface fully and tightly attached to measured skin regions and therefore background noise and signal leak were effectively reduced. The curved detector was made in a rigid circuit board design and hard encapsulated, which was easy to be held in hand and scan on the surface of the different measured body parts.

Within the above regime of the detector probe design, the signal to noise ratio is the key concern for the optoelectronic detector application. Here we address this issue by taking the most complicated structure body part head as an example. By using the approach of Monte Carlo light propagation modeling within multi-voxelized tissue media [18], we computed out signal sensitivity distribution (SSD) map (Figure 2(a)) within Visible Chinese Human [19,20,21] head model. SSD were shown in a pseudo color map with quantitative contours. The SSD data showed that the separation scale of the light source and detector approved the detectable depth within tissue to be more than 3 cm, when the signal to noise ratio was higher than the limit of the OPT101 sensor 1×10^{-7}. Plus, the accumulated light signal from the tissue region deeper than 3 cm was higher than 1.27×10^{-6} of the incident light, which also supported the sensitive and reliable sensing of light signal from the interrogated tissue volume by detector OPT101. In addition, with the usage of OPT101, fNIRS technology can be realized in a portable, small size, and compatible design.

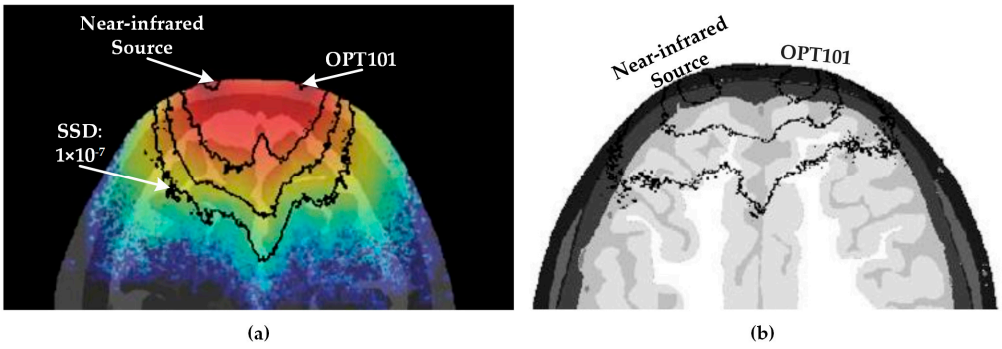

Figure 2. (**a**) Signal sensitivity contour map; (**b**) NIRS measurement sketch map.

2.2. Measurement algorithm of NIRS

By the principle that the hemoglobin are the main absorbers of the near-infrared light, the main chromosphere of human body water was almost transparent to near-infrared light, and different absorption spectrums of oxy- and deoxy- hemoglobin within near-infrared range, NIRS was capable of measuring hemodynamic variations with human tissue noninvasively. As shown in Figure 2(b), near-infrared source emitted light into tissue, and OPT101 received the light coming out from the tissue in the position which was distance (r_0) away from the light source. With different value of r_0, physiological parameters at different tissue layer were allowed to be extracted in our OPT 101 involved NIRS ICU-specific devices. In details, the detected light intensity (I) signal by OPT101 originated from the light traveling through the measured tissue was convert to optical density (OD) by the following equation:

$$OD = -\log\frac{I}{I_0} = -\log\frac{U}{U_0} \quad (1)$$

Where I_0 was the initial light intensity. U_0 and U were the initial converted voltage and the converted voltage signal responding to I_0 and I, respectively. By using the least square fitting method,

and treating the optical density as ordinate and the distance between source and sensor as abscissa, the relationship between the light diffusion factor at wavelength λ_i ($D(\lambda_i)$) and the slope ($S(\lambda_i)$) can be extracted as follows [9]:

$$D(\lambda_i) = 2.3S(\lambda_i) + D(SS) \quad (2)$$

Here, D(SS) was light diffusion factor of standard sample. And the absolute concentrations of HbO_2 ([HbO_2]) and Hb ([Hb]) were calculated by the following equations [9,16]:

$$C[HbO_2] = \frac{\varepsilon_{HbO_2}(\lambda_1)\mu_t'(\lambda_1)D^2(\lambda_2) - \varepsilon_{HbO_2}(\lambda_2)\mu_t'(\lambda_2)D^2(\lambda_1)}{3\mu_t'(\lambda_1)\mu_t'(\lambda_2)\ln 10[\varepsilon_{Hb}(\lambda_2)\varepsilon_{HbO_2}(\lambda_1) - \varepsilon_{Hb}(\lambda_1)\varepsilon_{HbO_2}(\lambda_2)]} \quad (3)$$

$$C[Hb] = \frac{\varepsilon_{Hb}(\lambda_1)\mu_t'(\lambda_1)D^2(\lambda_2) - \varepsilon_{Hb}(\lambda_2)\mu_t'(\lambda_2)D^2(\lambda_1)}{3\mu_t'(\lambda_1)\mu_t'(\lambda_2)\ln 10[\varepsilon_{Hb}(\lambda_2)\varepsilon_{HbO_2}(\lambda_1) - \varepsilon_{Hb}(\lambda_1)\varepsilon_{HbO_2}(\lambda_2)]} \quad (4)$$

Where $\varepsilon_{HbO_2}(\lambda_i)$ and $\varepsilon_{Hb}(\lambda_i)$ were the extinction coefficients of HbO_2 and Hb at wavelength λ_i, respectively. And in our applications, we utilized 735 nm and 850 nm for HbO_2 and Hb quantification. The light attenuation factor at wavelength λ_i, $\mu_t'(\lambda_i)$ was calculated by [9]:

$$\mu_t'(\lambda_i) = \frac{10^{\ln(\lambda_i)}\mu_t'(SS)[2.3S(\lambda_i) + D(SS) + (1/r_0)]}{D(SS) + (1/r_0)} \quad (5)$$

And $\mu_t'(SS)$ was the light attenuation of standard sample. And the [HbO_2] and [Hb] relative to the initial values ($\Delta[HbO_2]$ and Δ[Hb] respectively) were given below [9,22]:

$$\Delta[HbO_2] = \frac{\varepsilon_{Hb}(\lambda_1)\Delta\mu_a(\lambda_2) - \varepsilon_{Hb}(\lambda_2)\Delta\mu_a(\lambda_1)}{\varepsilon_{Hb}(\lambda_1)\varepsilon_{HbO_2}(\lambda_2) - \varepsilon_{Hb}(\lambda_2)\varepsilon_{HbO_2}(\lambda_1)} \quad (6)$$

$$\Delta[Hb] = \frac{\varepsilon_{HbO_2}(\lambda_2)\Delta\mu_a(\lambda_1) - \varepsilon_{HbO_2}(\lambda_1)\Delta\mu_a(\lambda_2)}{\varepsilon_{Hb}(\lambda_1)\varepsilon_{HbO_2}(\lambda_2) - \varepsilon_{Hb}(\lambda_2)\varepsilon_{HbO_2}(\lambda_1)} \quad (7)$$

Here, $\Delta\mu_a(\lambda)$ was the relative change of medium absorption coefficient at wavelength λ.

2.3. ICU-specific NIRS device and experiment test

The novel applications of OPT101 as photoelectric detector for ICU-specific NIRS device development in our lab were illustrated by thrombus diagnosis and monitoring, patient shock status monitoring, and fatigue evaluation in this paper. All these applications generated devices was consist of three parts, which were the flexible optical probe, control circuit module, and the computer included with control and data analysis software. The light source used was a 3-wavelengths (735 nm, 805 nm, and 850 nm) integrated LED. All the work of data collecting was approved by the ethics committee (Approval No. XHECD-2014-005).

2.3.1. Thrombus diagnosis and monitoring

Thrombus was a severe complication which can cause serious morbidity and mortality, usually happens in patients and those with postoperative population. Most patients with thrombus were at risk of developing post thrombotic dysfunctions, leading to long-term morbidity and induce ulceration, chronic swelling, skin damage, and other clinical manifestations. However, the conventional diagnosis relied on sophisticate imaging methodologies which might also induced invasive contrast agent injection and ionizing procedure. We proposed to develop a portable NIRS under patients' ease state for thrombus diagnosis, monitoring, and therapeutic effect evaluation [15,17].

Preprints (www.preprints.org) | NOT PEER-REVIEWED | Posted: 26 April 2017 doi:10.20944/preprints201704.0166.v1

Peer-reviewed version available at Sensors 2017, 17, 1701; doi:10.3390/s17081701

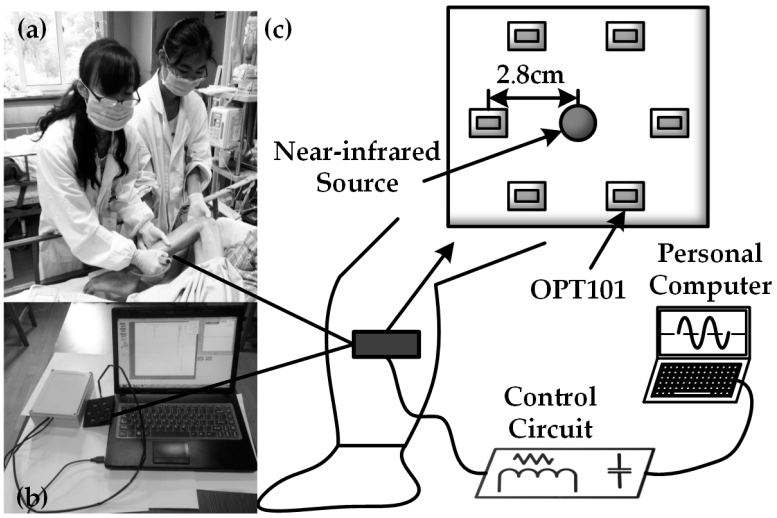

Figure 3. Thrombus diagnosis: **(a)** data collection scene; **(b)** actual device for thrombus; **(c)** connection diagram.

The OPT101 embedded NIRS device was shown in Figure 3. Figure 3(a) showed the real scene where we collected the data from a patient suffering from thrombus on clinic field monitoring. Figure 3(b) showed our custom device design and Figure 3(c) showed the placement of the light source and detector in the probe. Figure 3(a) also illustrated the use of the device. The probe included one light source and six detectors surrounded. The light source and detector were driven by a control circuit module to emit 735 nm and 850 nm light and collect signals from the OPT101s at a set timing sequence. The distance between light source and OPT101 detector was 2.8 cm, enabling most signal coming from the muscle layer in the early thrombus body part, such us legs and arms. We attempted to explore if $\Delta[HbO_2]$ and $\Delta[Hb]$ could reflect the occurrence or state of thrombus.

We collected data from 9 patients with thrombosis during and after therapy. We also collected data from 7 healthy doctor for contrast. We analyzed these data and drew the scatterplot histograms of $\Delta[HbO_2]/\Delta[Hb]$ for statistical comparisons between both populations. Thrombolytic therapy lasted for 1 day. With data collected the NIRS monitoring data during therapy observation time every day until the patients recovered (six times totally), we obtained $\Delta[HbO_2]$ along with days during therapy between healthy and thrombus legs.

2.3.2. Monitoring patients with shock

Shock usually caused acute blood flow reduction, anaerobic metabolism, cellular and organ dysfunction, and irreversible damage and death if sustained. The inevitable hemorrhage during surgery and traumatic injury induced shock was known as a fatal complication with ~50% in mortality [16]. The conventional clinical method to estimate shock severity was to measure blood sample oxygen indices in the central internal jugular central vein, which was abbreviated as $ScvO_2$. However, the intermittent and invasive procedures to obtain this acceptable blood oxygen indicator actually denied continuous shock monitoring, which was crucial for clinicians to catch the best time window to rescue the patient. We developed a portable spatially-resolved NIRS device for bedside monitoring of patients with shock.

In this application, we recommended the tissue blood oxygen saturation (StO_2) measured in the tissue surrounding the central internal jugular central vein as indicator for shock severity. And the value of StO_2 was calculated by $[HbO_2]$ and [Hb] as follows:

$$StO_2 = \frac{C[HbO_2]}{C[HbO_2] + C[Hb]} \times 100\% \quad (8)$$

Compared to thrombus diagnosis, the NIRS monitor for patients with shock (Figure 4(a)) offers the measure of physiological parameters in the lateral neck region (Figure 4(c)). The design of flexible optical probe was space-resolved (Figure 4(b)), allowing absolute measure of $[HbO_2]$ and [Hb]. Figure 4(a) showed the device for shock monitoring.

Peer-reviewed version available at Sensors 2017, 17, 1701; doi:10.3390/s17081701

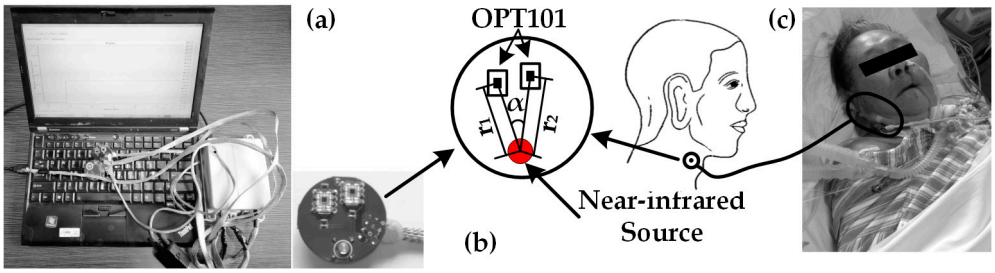

Figure 4. Shock monitoring: **(a)** actual device for shock; **(b)** the probe for shock; **(c)** picture of clinical experiment test scene

There were one near-infrared light source and two detectors on the probe of the monitor for patients with shock. The distance between the light source and the two OPT101 were slightly different, r_1 and r_2 respectively. The angle from one detector to the other regarding the source point as the center was α. The value of α varies at the range of 0 to 13.5°. And the typical value of the angle was between 4.5° and 9.5°. The set of angle was due to the two restrictions, which were the safe distance between OPT 101 and slight difference between r_1 and r_2. With differential set of r_1 and r_2, as well as the absolute measure algorithm, we were able to obtain the measure of the StO_2 in the shock-status-sensitive region, the tissue surrounding the central internal jugular central vein. We acquired data from 12 patients one day after shock treatment. For comparison, we not only analyzed StO_2, but also $ScvO_2$ which was a golden standard indicator for shock prediction, by linear analysis and Bland-Altman plot [16].

2.3.3. Fatigue evaluation

The doctors and nurses always work long in the intensive care unit, accordingly the fatigue became a severe problem requiring quantitative management and proper intervention. Here we focused on the prolonged work or operation induced fatigue. Computer game playing paradigm was used to mimic the ICU clinicians' working fatigue. We recruited 10 healthy subjects to play computer games for 7 hours with a realistic driving simulator platform as shown in Figure 5(a). Subjects were instructed to take visual selective attention test every one hour during the whole 7 hours' computer game. We collected brain activities data with a portable NIRS imager (probe shown in Figure 5(b)) attached on the subjects' foreheads at the beginning of driving and then every 1 hour (Figure 5(a)). The brain activity response was interpreted by hemodynamic recordings ($[HbO_2]$ and [Hb]) based on the neurovascular coupling theory. The data of variations of $[HbO_2]$ and [Hb] recorded in the attention test was used to test if it can be used for fatigue evaluation. As shown in the Figure 5(b), the probe of fatigue evaluation contains a near-infrared light source and 20 detectors, which composed 8 channels' detection and allowed reducing artifact from skin by the nearest detector to the source and absolute measures of $\Delta[HbO_2]$ and Δ[Hb]. Figure 5(c) showed the picture of our custom NIRS device for fatigue evaluation.

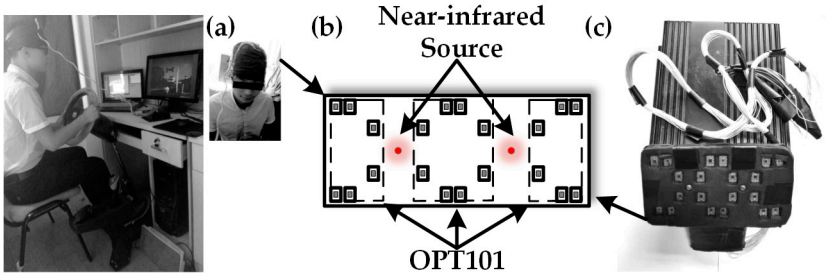

Figure 5. Fatigue evaluation: **(a)** data collection scene; **(b)** the probe for fatigue; **(c)** actual device.

During NIRS data recording, we also recorded the response of subjects to the attention stimuli on keyboard and reaction time. For data analysis, we composited the mean behavioral factor from 10 subjects at every attention test as accuracy/RT to quantify the mental fatigue of subjects. Then we

analyzed the relationship between the hemodynamic parameters and the behavioral data accuracy/RT following with the fatigue increment induced by computer game playing. We also computed the prefrontal activation map with fatigue degree increase for intuitively visualizing fatigue adjustment on prefrontal activity.

3. Results

3.1. Thrombus diagnosis and therapeutic effect evaluation

Figure 6(a) showed comparison of the composed hemodynamic parameter $\Delta[HbO_2]/\Delta[Hb]$ between normal subjects and thrombus patients. In general, the value of $\Delta[HbO_2]/\Delta[Hb]$ of normal subjects (11.0 ± 0.95) were higher than those of thrombus patients (9.6 ± 1.10). Student T-test also showed that the above measurements are dramatically different between normal subjects and thrombus patients ($p<0.001$). One other side, Figure 6(b) showed the hemodynamic response to therapeutic effect. The value of $\Delta[HbO_2]$ in thrombus legs decreases after therapy, and increases gradually during recovery phase and finally reach a significantly higher value after two days since treatment. And for healthy leg, the value of $\Delta[HbO_2]$ recovered to the initial state in one day and then remains stable after the therapy. Accordingly, the hemodynamic response monitored by our noninvasive NIRS thrombus monitor was shown to be capable of differentiating thrombus region from health region of human body and evaluating the therapeutic effect, no matter composed hemodynamic parameter ($\Delta[HbO_2]/\Delta[Hb]$) or the relative more sensitive indicator ($\Delta[HbO_2]$).

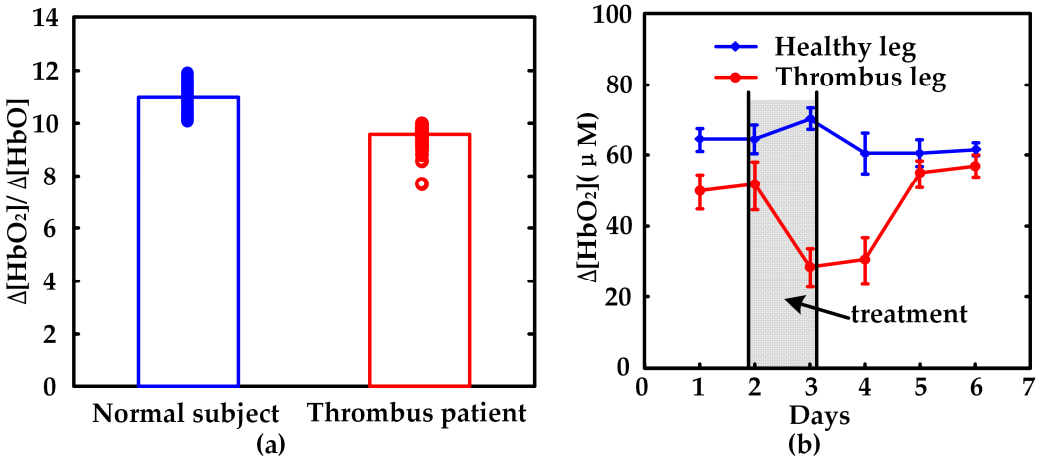

Figure 6. Measurements on thrombus clinics: **(a)** comparison of $\Delta[HbO_2]/\Delta[Hb]$ between normal subjects and thrombus patients; **(b)** the variation of $\Delta[HbO_2]$ along with days between healthy leg and thrombus leg.

3.2. Monitoring patients with shock

As a gold standard indicator for prediction of shock severity, $ScvO_2$ data was also collected by the conventional blood drop sampling and blood-gas analysis for each subject during the experiment. $ScvO_2$ was employed as a contrast to test if StO_2 measured by NIRS shock monitor was reliable and sensitive to monitor shock severity. Figure 7(a) showed a significant linear regression between StO_2 and $ScvO_2$. The correlation coefficient between the results of StO_2 and $ScvO_2$ was high ($R=0.843$, $p<0.001$). As shown in Figure 7(b), there were only three data points out of the total 12 data which fell over the 95% confidence interval for StO_2. However, those three data points were quite close to the 95% confidence interval. Figure 7(c) was the Bland-Altman plot for StO_2 and $ScvO_2$, which clearly illustrated that there exists a pretty agreements between these two parameters (the mean difference is 4.16%). It indicated that StO_2 measured in the $ScvO_2$ origin site of human body by NIRS is potential to substitute the current golden standard $ScvO_2$.

Preprints (www.preprints.org) | NOT PEER-REVIEWED | Posted: 26 April 2017 doi:10.20944/preprints201704.0166.v1

Peer-reviewed version available at Sensors 2017, 17, 1701; doi:10.3390/s17081701

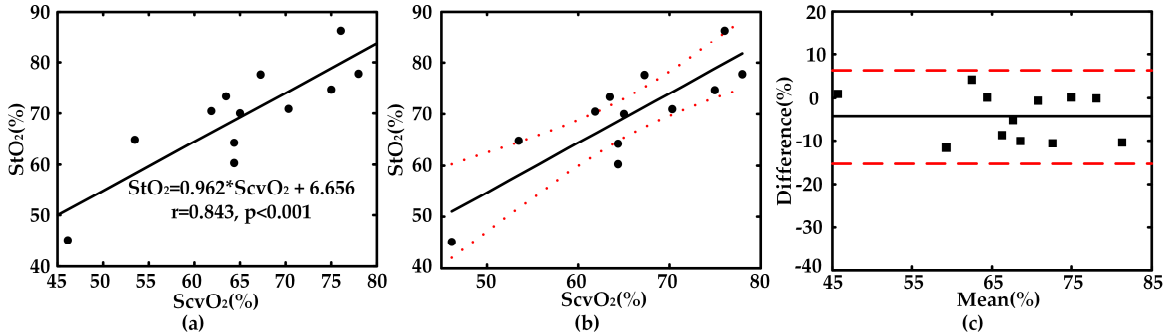

Figure 7. Comparison between StO_2 and $ScvO_2$: **(a)** linear analysis; **(b)** 95% confidence interval for StO_2 (dot line); **(c)** difference plot and 95% limits of an agreement (dash line).

3.3. Fatigue evaluation and data

As for fatigue evaluation, Figure 8 showed that both the prefrontal activity induced $\Delta[HbO_2]$ measured by NIRS imager and the behavioral performance factor accuracy/RT both varied nonlinearly along with time duration of playing computer game. Figure 8(a) displayed the prefrontal activation map following with continuous computer game duration. The pseudo color map presented the amplitude of the activation increases gradually in the prefrontal lobe and especially in the middle bottom prefrontal region, which was highlighted in the black rectangular box in the map (Figure 8(a)). After we extracted the mean value of brain activation in terms of $\Delta[HbO_2]$ of every subject, we plotted its variation with duration time statistically, as well as the behavioral performance. We found that the fatigue-induced $\Delta[HbO_2]$ rise up while fatigue-induced behavioral performance fell down in a similar opposite tendency (Figure 8(b)). Interestingly, the statistical mean $\Delta[HbO_2]$ and accuracy/RT showed a strong negative linear correlation (R=-0.896, p=0.002).

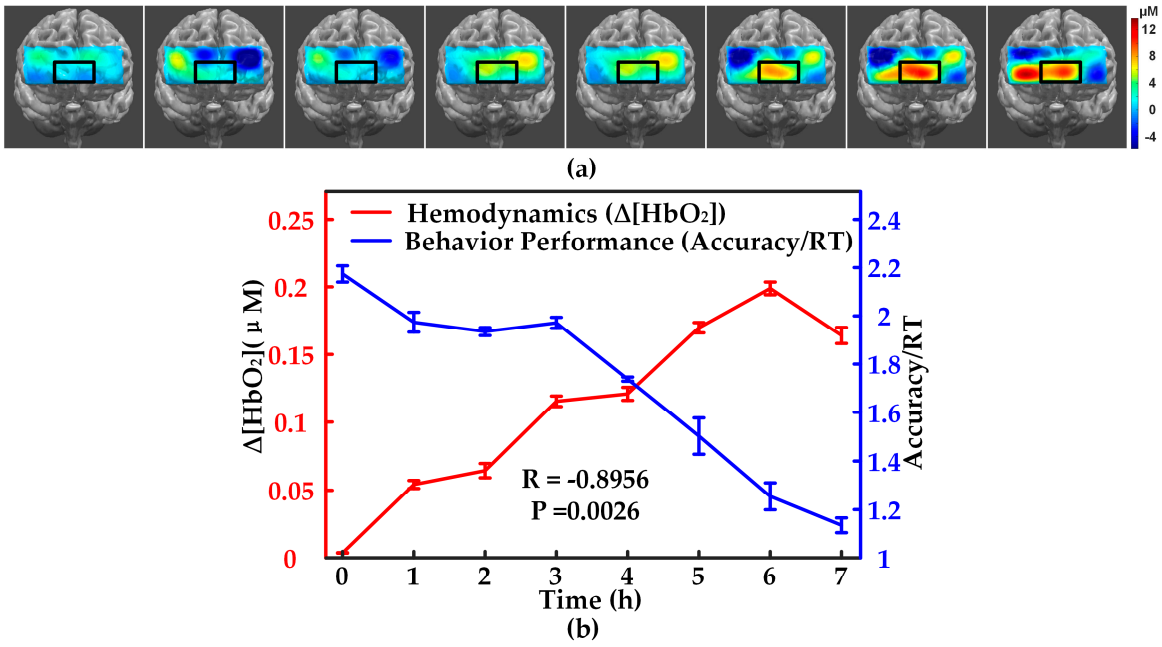

Figure 8. Fatigue measurements: **(a)** prefrontal activation map variation along with computer game duration; **(b)** $\Delta[HbO_2]$ increment and behavioral performance factor along with computer game duration.

4. Conclusion and Discussion

With the optoelectronic detector OPT101, we innovatively developed a series of NIRS devices for intensive care unit, including the common heath scanner, the thrombus monitor, monitor for patients with shock, and the imager for fatigue evaluation. All of these device were noninvasive,

portable, small-size, and real time. These devices surpassed the current methodologies or conventional techniques used in those severe diseases in mainly noninvasive, nonionizing, and continuous measurements. The experiment studies of each device displayed good reliability and sensitivity. The whole study fully demonstrated the medical and life science application of OPT101 with the regime of near-infrared spectroscopy, and indicate the great potential of OPT101, as well as the OPT101 imbedded portable NIRS, in ICU and respective home health.

Our study on thrombus monitor showed that NIRS monitoring of $\Delta[HbO_2]/\Delta[Hb]$ played pretty sensitive role in diagnosis of thrombus, as well as the therapeutic effect tracking and evaluation. Of note, the monitor probe was applicable to the early thrombosis body parts, such as the legs, which indicated the home care use of this device in early detection and development of thrombosis. In the application of monitoring patients with shock, we found that the StO_2 measured in the tissue surrounding the central jugular vein is quite consistent with the golden standard indicator $ScvO_2$, which was measured by blood drop sampling and blood-gas analysis. Apparently, the $ScvO_2$ could not be measured continuously and real time, which actually was not possible to monitoring shock and to predict the time window for rescuing the patients. On the contrast, StO_2 measured by NIRS shock monitor was quite proper for monitoring the coming of the shock and severity change of the shock. As for fatigue evaluation, the variation $\Delta[HbO_2]$ measured by the NIRS fatigue imager increased with the working time and were highly negatively correlated with fatigue-adjusted behavioral performance score ($R=-0.899$, $p=0.0026$). This finding strongly supported the quantitative evaluation of fatigue in a noninvasive and in-situation way by NIRS.

In the future, we will expand the range of OPT101-imbeded NIRS for more applications. However, OPT101 is expected to be realized in patch type design in the future, which would allow the flexible and wearable design of the above NIRS devices for more convenient medical applications.

Acknowledgments: We thanked all subjects in this research for their sincere support and effective cooperation. We appreciate the supports of the One University One Zone Growth Fund (No.A03013023001019), and National Natural Science Fund Projects (No.61675039). We also thank Daniel Hines, MS, for his generous assistance in language improvement.

Author Contributions: Ting Li conceived the idea of this study and collected the data. Fulin Zhong, Boan Pan and Zebin Li analyzed the data and processed the figures. Ting Li, Fulin Zhong, and Zishan Deng wrote this article.

Conflicts of Interest: The authors declare no conflict of interest.

References

1. Romeira, B.; Pessoa, L. M.; Salgado, H. M.; Ironside, C. N.; Figueiredo, J. M. Photo-detectors integrated with resonant tunneling diodes. *Sensors* **2013**, *13(7)*, 9464–9482, DOI: 10.3390/s130709464.
2. Thalheimer, M. A new optoelectronic sensor for monitoring fruit or stem radial growth. *Computers & Electronics in Agriculture* **2016**, *123(C)*, 149-153, DOI: 10.1016/j.compag.2016.02.028.
3. J. Wojtas, Z; Bielecki, J; Mikolajczyk; T. Stacewicz. (2013). P2.5 - high sensitivity optoelectronic sensor for nitric oxide detection in exhaled air. AMA Conferences 2013, Nürnberg, 14-16 May 2013, Proceedings SENSOR 2013 Vol. 724 – 727, DOI: 10.5162/sensor2013/P2.5.
4. Lochner, C. M.; Khan, Y.; Pierre, A.; Arias, A. C. All-organic optoelectronic sensor for pulse oximetry. *Nature Communications* **2014**, *5*, 5745, DOI: 10.1038/ncomms6745.
5. Zilberman, Y.; Sonkusale, S. R. Microfluidic optoelectronic sensor for salivary diagnostics of stomach cancer. *Biosensors & Bioelectronics* **2014**, *67*, 465-471, DOI: 10.1016/j.bios.2014.09.006.
6. Pedowitz, R.A.; Shackford S. R. Non-cavitary hemorrhage producing shock in trauma patients: incidence and severity. *Journal of Trauma* **1989**, *29(2)*, 219–222, DOI: 10.1097/00005373-198902000-00012.
7. Peitzman, A.B.; Harbrecht, B.G.; Udekwu, A.O.; Billiar, T. R.; Kelly, E.; Simmons R.L. Hemorrhagic shock. *Current Problems in Surgery* **1995**, *32(11)*, 925–1002, DOI: 10.1016/S0011-3840(05)80008-5.
8. Mino, J.S.; Gutnick, J.R.; Monteiro, R.; Anzlovar N.; Siperstein A.E. Line-associated thrombosis as the major cause of hospital-acquired deep vein thromboses: an analysis from National Surgical Quality Improvement Program data and a call to reassess prophylaxis strategies. *American journal of surgery* **2014**, *208(1)*, 45–49, doi: 10.1016/j.amjsurg.2013.08.046.

9. Li, T.; Zhao, Y.; Sun, Y.; Gao, Y.; Su, Y.; Hetian, Y.; Chen M. Near-infrared spectroscopy assessment of divided visual attention task-invoked cerebral hemodynamics during prolonged true driving. SPIE BiOS. International Society for Optics and Photonics.. Near-infrared spectroscopy assessment of divided visual attention task-invoked cerebral hemodynamics during prolonged true driving. SPIE BiOS International Society for Optics and Photonics, The Moscone Center, San Francisco, California, USA, 7–8 February 2015; Henry Hirschberg, Steen J. Madsen, Eds; SPIE Proceedings Vol. 9305: 2015.
10. Li, Z.; Zhang, M.; Zhang, X.; Dai, S.; Yu, X; Wang, Y. Assessment of cerebral oxygenation during prolonged simulated driving using near infrared spectroscopy: its implications for fatigue development. *European Journal of Applied Physiology* **2009**, *107(3)*, 281-287, doi: 10.1007/s00421-009-1122-6.
11. Boas, D.A.; Pitris, C.; Ramanujam, N. In *Handbook of Biomedical Optics*, page 831, CRC Press: Hoboken, NJ, 2011; Volume 10, pp. 195–216.
12. Dale, L. M.; Thewis, A.; Rotar, I.; Pierna, J. A. F.; Boudry, C.; Vidican, R. M. Chemometric tools for nirs and nir hyperspectral imaging. *Bulletin of Usavm Cluj Napoca Agriculture* **2012**, *69(1)*, 70-76, Available online: http://journals.usamvcluj.ro/index.php/agriculture/article/viewFile/8658/7332.
13. Teye, E.; Huang, X.; Afoakwa, N. Review on the potential use of near infrared spectroscopy (nirs) for the measurement of chemical residues in food. *American Journal of Food Science & Technology* **2013**, *65(1)*, 661-668, DOI: 10.12691/ajfst-1-1-1.
14. Boyer, C.; Gaudin, K.; Kauss, T.; Gaubert, A.; Boudis, A.; Verschelden, J.; Franc, M.; Roussille, J.; Boucher J.; Olliaro, P.; White, N.J.; Millet, P.; Dubost, J.P. Development of nirs method for quality control of drug combination artesunate-azithromycin for the treatment of severe malaria. *Journal of Pharmaceutical & Biomedical Analysis* **2011**, *67-68(100)*, 10-15, DOI: 10.1016/j.jpba.2012.04.009.
15. Li, T.; Sun, Y.; Chen, X.; Zhao, Y.; Ren, R. Noninvasive diagnosis and therapeutic effect evaluation of deep vein thrombosis in clinics by near-infrared spectroscopy. *Journal of Biomedical Optics* **2015**, *20(1)*, 010502, DOI:10.1117/1.JBO.20.1.010502.
16. Li, T.; Duan, M.; Li, K.; Yu, G.; Ruan, Z. Bedside monitoring of patients with shock using a portable spatially-resolved near-infrared spectroscopy. *Biomedical Optics Express* **2015**, *6(9)*, 3431-3436, doi:10.1364/BOE.6.003431.
17. Li, T.; Sun, Y.; Chen, X.; Zho, Y.; Ren, R; Liu, M. Non-invasive diagnosis and continuous monitoring of thrombosis in clinics by near-infrared spectroscopy. SPIE BiOS International Society for Optics and Photonics, The Moscone Center, San Francisco, California, USA, 7–8 February 2015; Anita Mahadevan-Jansen, Tuan Vo-Dinh, Eds; SPIE Proceedings Vol. 9313: 2015.
18. Li, T.; Gong, H.; Luo, Q. MCVM: MONTE CARLO MODELING OF PHOTON MIGRATION IN VOXELIZED MEDIA. *Journal of Innovative Optical Health Sciences* **2011**, *3(2)*, 91-102, DOI: 10.1142/S1793545810000927.
19. Zhang, G.; Luo, Q. S.; Liu, Q. The development and application of the visible chinese human model for monte carlo dose calculations. *Health Physics* **2008**, *94(2)*, 118, DOI: 10.1097/01.HP.0000285256.48498.b4.
20. Zhang, S. X.; Heng, P. A.; Liu, Z. J.; Tan, L. W.; Qiu, M. G.; Li, Q. Y. The chinese visible human (cvh) datasets incorporate technical and imaging advances on earlier digital humans. *Journal of Anatomy* **2004**, *204(3)*, 165, DOI: 10.1111/j.0021-8782.2004.00274.x.
21. Li, T.; Gong, H.; Luo, Q. Visualization of light propagation in visible chinese human head for functional near-infrared spectroscopy. *Journal of Biomedical Optics* **2011**, *16(4)*, 045001, DOI: 10.1117/1.3567085.
22. Li, T.; Lin, Y.; Yu, S.; He, L.; Huang, C.; Szabunio, M. Simultaneous measurement of deep tissue blood flow and oxygenation using noncontact diffuse correlation spectroscopy flow-oximeter. *Scientific Reports* **2013**, *3(1)*, 1358, DOI: 10.1038/srep01358.